PCCP

Accepted Manuscript

ROYAL SOCIETY OF CHEMISTRY

www.rsc.org/pccp

Photophysical, amplified spontaneous emission and charge transport properties of oligofluorene derivatives in thin films

E.Y. Choi,[1] L. Mazur,[2,3] L. Mager,[4] M. Gwon,[1] D. Pitrat,[5] J.C. Mulatier,[5] C. Monnereau,[5] A. Fort,[4] A.J. Attias,[2] K. Dorkenoo,[4] J. E. Kwon,[6] Y. Xiao,[2] K. Matczyszyn,[3] M. Samoc,[3] D.-W. Kim,[1] A. Nakao,[7] B. Heinrich,[4] D. Hashizume,[8] M. Uchiyama,[9,10] S. Y. Park,[6] F. Mathevet,[2] T. Aoyama,[9] C. Andraud,[5] J.W. Wu,[1] A. Barsella,[4] J. C. Ribierre[1]*

[1] Department of Physics, CNRS-Ewha International Research Center, Ewha Womans University, Seoul, South Korea

[2] Institut Parisien de Chimie Moléculaire, Chimie des Polymères, Université Pierre et Marie Curie, UMR 8232, 3 rue Galilée, Ivry, France

[3] Institute of Physical and Theoretical Chemistry, Wroclaw University of Technology, Wybrzeze Wyspianskiego 27, 50-370 Wroclaw, Poland

[4] Institut de Physique et Chimie des Matériaux de Strasbourg (IPCMS), UMR 7504, CNRS-Université de Strasbourg, 23 rue du Loess, 67034 Strasbourg Cedex 2, France

[5] CNRS-UMR 5182, University of Lyon 1, Ecole Normale Supérieure de Lyon, 46 avenue d'Italie, Lyon, France

[6] Department of Materials Science and Engineering, Seoul National University, Seoul, South Korea

[7] Nuclear Spectroscopy Laboratory, RIKEN Nishina Center for Accelerator-Based Science (RNC), 2-1 Hirosawa, Wako, Japan

[8] Materials Characterization Support Unit, RIKEN Center for Emergent Matter Science (CEMS), 2-1 Hirosawa, Wako, Japan

[9] Elements Chemistry Laboratory, RIKEN, 2-1 Hirosawa, Wako, Japan

[10] Graduate School of Pharmaceutical Sciences, The University of Tokyo, 7-3-1 Hongo, Bunkyo-ku, Tokyo 113-0033, Japan

ABSTRACT

We investigate the photophysical and amplified spontaneous emission properties of a series of monodisperse solution-processable oligofluorenes functionalized with hexyl chains at the C9 position of each fluorene unit. Thin films of these oligofluorenes are then used in organic field-effect transistors and their charge transport properties are examined. We have particularly focused our attention on the influence of oligofluorene length on the absorption and steady-state fluorescence spectra, on the HOMO/LUMO energy levels, on the photoluminescence lifetime and quantum yield as well as on the amplified spontaneous emission properties and the charge carrier mobilities. Differential scanning calorimetry and X-ray diffraction measurements demonstrate that, among all oligofluorene derivatives used in this study, only the structure and morphology of the pentafluorene film is significantly modified by a thermal treatment above the glass transition temperature, resulting in a 9 nm blue-shift of the fluorescence spectrum without significant changes in the photoluminescence quantum yield and in the amplified spontaneous emission threshold. In parallel, hole field-effect mobility is significantly increased from 8.6 x 10^{-7} to 3.8 x 10^{-5} cm^2 V^{-1} s^{-1} upon thermal treatment, due to an increase of crystallinity. This study provides useful insights into the morphological control of oligofluorene thin films and how it affects their photophysical and charge transport properties. Moreover, we provide evidence that, because of the low threshold, the tunability of the amplified spontaneous emission and the photostability of the films, these oligofluorenes are promising candidates for organic solid-state laser applications.

Keywords: Oligofluorene, conjugation length, film morphology, amplified spontaneous emission, organic field-effect transistor

1. INTRODUCTION

Polyfluorenes and oligofluorenes are nowadays considered as a promising class of organic semiconducting molecules for a range of optoelectronic applications including organic light-emitting diodes (OLEDs), organic solid-state lasers and sensors.[1-12] These materials generally present good charge transport properties with an ambipolar character[13-15], display excellent thermal and oxidative stability[16], show blue emission with high photoluminescence quantum yield (PLQY) and high laser gain.[17] Due to their wide bandgap, fluorene derivatives have been used in blue, green and red OLEDs as host material for fluorescent and phosphorescent guest molecules.[18,19] These materials have been also successfully used in one- and two-photon pumped solid-state lasers[20,21] and optical amplifiers.[22] Most of these compounds are soluble in common organic solvents and thus can be readily processed from solution into semiconducting thin films by spin-coating or inkjet printing techniques, which is a key-feature for low-cost and large-area optoelectronic devices. Another important feature of these fluorene derivatives is their rich polymorphic behavior.[23-25] For example, poly(9,9-dioctyl)fluorene (PFO) is known to exhibit at least three different phases in thin films, which can be achieved by some specific thermal or solvent vapor treatments.[24,25] It has also been demonstrated that monodisperse oligofluorenes with thermotropic nematic mesomorphism can be uniaxially aligned on a rubbed surface, resulting in a strong polarization of the emitted light in OLEDs and an enhancement of the charge carrier mobilities in organic field-effect transistors (OFETs).[26-28] Despite a large number of studies devoted to morphological effects in polyfluorene and oligofluorene thin films, a better understanding of the structure-to-property correlations in these materials is still required for further improvement of their optoelectronic performances.

In this manuscript, we present a study on the structural, morphological, photophysical, amplified spontaneous emission and charge transport properties of oligofluorene thin films. As shown in Fig.1, all the oligofluorene derivatives used in this work are functionalized with hexyl chains at the C9 position of each fluorene unit. Our results clarify the role played by the oligofluorene length on their fluorescence, amplified spontaneous emission (ASE) and charge transport properties. While the as-spin-coated oligofluorene thin films are amorphous, we found that morphological effects take place upon a thermal annealing above the glass transition temperature (T_g) specifically in the pentafluorene film, providing a scope for fine tuning of the

emission without significant changes in PLQY and ASE performances. Bottom-gate, bottom-contact OFETs based on pentafluorene thin films were fabricated in order to explore the influence of the changes in molecular packing caused by the annealing on the charge transport properties. An increase of the hole mobility by almost two orders of magnitude is evidenced in the annealed films. We attribute this enhancement to the increase of crystallinity and a more favorable molecular packing. Overall, this work shows that the investigated oligofluorene derivatives are interesting candidates for organic solid-state laser applications. In particular, it provides useful insights into the control of film morphology and its implications on the optoelectronic properties of fluorene derivatives.

2. EXPERIMENTAL SECTION

The heptafluorene material was purchased from American Dye Source. The other oligofluorene derivatives were synthesized following a method previously published in the literature.[29] Thin films for the photophysical measurements were prepared from chloroform solutions and were spin-coated onto precleaned fused silica substrates. Absorption and photoluminescence (PL) spectra of the films were obtained by a UV-visible-near infrared absorption spectrophotometer (Shimadzu UV-3100PC) and a steady-state spectrofluorimeter (Shimadzu RF-5301F), respectively. The PLQY in film was measured by a PTI QuantaMaster 40 spectrophotometer equipped with a 3.2-inch integrating sphere. In our experiments, we used the excitation wavelength of 350 nm for the terfluorene films and of 370nm for the pentafluorene and the heptafluorene films. The time-resolved photoluminescence measurements were performed using a PicoQuant FluoTime 200 spectrophotometer by exciting samples with 44ps pulses at 377nm with a repetition rate of 10MHz. For the photophysical measurements in solution, oligofluorenes were dissolved in chloroform. Absorption and PL spectra were recorded using a Jasco 670 UV-Visible spectrometer and a Horiba-Jobin Yvon Fluorolog-3® spectrofluorimeter respectively. The solution PLQY value of oligofluorenes was evaluated using quinine sulfate in 0.1 M sulfuric acid (PLQY of 55 %) as a reference. The PL decays in solution were measured using the Horiba-Jobin-Yvon Fluorolog-3® spectrofluorimeter, equipped with a NanoLED 390L source operating at 390 nm with 250 ps pulses, an iHR320 emission monochromator with 1200 groves/mm gratings and a R928 detector. All the photoluminescence measurements in both solution and films were carried out at room temperature.

Oligofluorene films for the ASE measurements were prepared by spin-coating from chloroform solution with a concentration in the range of 20~25 mg/ml. The samples were pumped at 325 nm with a femtosecond laser source (Spectra Physics, MaiTai-Spitfire-TOPAS OPA) delivering ~80 fs duration pulses, at 5 kHz. The excitation wavelength of 325 nm was obtained from the fourth harmonic of an optical parametric amplifier output centered at 1300 nm. A cylindrical lens was employed to focus the excitation beam into a stripe of dimensions 0.2 x 7 mm^2. The emission spectra were measured as a function of the pumping intensity from the edge of the films using an optical fiber, which was coupled to a CCD spectrometer (Ocean Optics HR4000CG-UV-NIR).

Charge transport properties of the oligofluorene derivatives were investigated by organic field-effect transistor (OFET) measurements. The experiments were performed on solution-processed thin films fabricated in a glove-box filled with nitrogen gas. For this purpose, bottom-gate bottom-contact OFETs were fabricated on silicon wafers with a thermally grown 280 nm SiO_2 layer (MicroChemicals GmbH). Interdigitated source and drain electrodes were prepared by photolithography and were achieved by the sequential thermal evaporation of a 5 nm thick adhesion layer of Ti and a 100 nm Au layer. The channel length and width was 5 μm and 1.9 cm, respectively. The substrates were cleaned by sonication in acetone and isopropanol baths, followed by UV-ozone treatment (ProCleaner™, BioForce Nanosciences). The terfluorene, pentafluorene and heptafluorene derivatives were dissolved in chloroform at a concentration of 5 mg/ml in N_2 atmosphere. Films were then spin-coated from these solutions at a spin speed of 3000 rpm. The current-voltage characteristics of these devices were finally recorded in inert atmosphere using an MS-Tech MST8000C probe station combined with a Keithley 4200 Semiconductor Characterization System.

The thermal phase transitions of the oligofluorene derivatives were analyzed by differential scanning calorimetry (DSC) using TA instruments Q2000 under N2 flow in hermetic aluminum pans. Atomic force microscopy (AFM) measurements were carried out using a scanning probe microscope (Veeco D3100 AFM) in the tapping mode. The X-ray diffraction (XRD) measurements in films were performed using an X-ray diffractometer (SmartLab, Rigaku) in the conventional θ-2θ configuration using Cu Kα1 radiation emitting at 1.54056 Å.

The XRD measurements in the bulk were performed on samples filled in Lindemann capillaries, with a home-built set-up using a linear monochromatic Cu Kα1 beam from a sealed-tube generator, equipped with a bent quartz monochromator, a home-built oven and a curved Inel CPS 120 gas-filled detector. Grazing incidence wide angle x-ray scattering (GIWAXS) measurements were carried out at PLS-II 9A U-SAXS beamline of Pohang Accelerator Laboratory (PAL) in Korea. For these experiments, oligofluorene films were spin-coated on silicon and fused silica substrates. The x-rays coming from the vacuum undulator (IVU) were monochromated using Si(111) double crystals and focused on the detector using K-B type mirrors. Patterns were recorded with a 2D CCD detector (Rayonix SX165). The sample-to-detector distance was about 221 mm for energy of 11.105 keV (1.1165 Å).For the determination of the ionization potential in thin films, UV photoelectron spectroscopy (UPS) measurements were performed in oligofluorene thin films thinner than 20 nm and deposited onto indium tin oxide (ITO) glass substrates. These experiments were carried out using an ESCALAB 250 (Thermo Fisher Scientific K.K.) system with monochromatized HeI (21.2 eV) as photon source. During these measurements, the samples were biased at -5 V.

Quantum chemistry calculations were performed using the RIKEN Integrated Cluster of Clusters (RICC) facility to determine the electronic properties of the oligofluorenes including the gap energies between the highest occupied molecular orbital (HOMO) and the lowest unoccupied molecular orbital (LUMO) as well as the frontier orbital distributions. The optimized molecular structures and the frontier molecular orbitals of the oligofluorenes were computed at the B3LYP/6-311G(d,p) level with the Gaussian 09 suites of programs.[30] Note that the alkyl side-chains were removed from the oligofluorene structures to reduce the computational load.

3. RESULTS

3.1 Thermal and structural properties

The thermal phase transitions of the oligofluorenes were examined by DSC measurements. As shown in Fig. 2, five consecutive heating/cooling cycles were measured in ter-, penta- and heptafluorene from 0 to 200 ºC at decreasing rates from 20°C/min to 2°C/min. Concerning the pentafluorene (Fig. 2a), the first heating DSC trace of the pristine material shows

a glass transition at about 57 °C, a broad exothermic peak from 100 °C to 140 °C (ΔH≈ –46 J/g) attributed to a cold crystallization and a sharp endothermic peak of the same area (ΔH≈ 46 J/g) corresponding to the melting of the just obtained crystalline phase. Down to rates of 2°C/min, the semi-crystalline state never restores on cooling, but cold crystallization occurs again on further heatings (at 5°C/min and 2°C/min) with crystallinities increasing logically with decreasing heating rate. Similar experiments were carried out with the terfluorene and heptafluorene derivatives. Concerning the terfluorene (Fig. 2b), the first DSC trace on heating shows a large endothermic peak at around 85 ºC (ΔH≈57 J/g) corresponding to a melting of the crystalline fraction in the pristine material. Further cooling and heating cycles never restored the semi-crystalline state, the terfluorene staying an amorphous material with a glass transition at around 25 ºC. Concerning the heptafluorene (Fig. 2c), the DSC traces show only a glass transition at around 60 ºC already on first heating, indicating that this material is steadily amorphous.

X-ray diffraction experiments were carried out on the oligofluorene thin films in the specular plane to gain insights into their morphology. As shown in Fig. 3, the absence of sharp peaks in the X-ray diffraction patterns of the as-prepared heptafluorene and pentafluorene deposits is consistent with the fully amorphous structure of these bulk oligomers in the pristine state. In consistency with DSC results, further thermal processing of the heptafluorene film leaves this morphology (and thus the diffraction pattern after annealing at 100°C) unchanged (Fig. 3c). In contrast, a sharp small-angle reflection appears in the X-ray diffractogram of pentafluorene film after annealing at 100°C, which is likely related to crystallization, in agreement with previous results on bulk pentafluorene[31] and with the DSC trace. The completion of the cold crystallization process during annealing at 100°C was finally confirmed with transmission diffraction experiments in temperature (Fig. 3b). The dominant reflection at 16.1 Å in this pattern moreover coincides with the single reflection observed for the film and indicates that crystallites of the same phase grow in the whole film but with a determined orientation with respect to the film surface. The microstructure of the pentafluorene thin films was also studied using 2D grazing incidence X-ray scattering (GIXS) on a synchrotron line. The two-dimensional GIXS images of pentafluorene as-prepared and annealed films are given respectively in Fig. 4a and Fig. 4b. These patterns show clearly the crystallization of the pentafluorene films after annealing at 100°C, with the reflection at 16.1 Å and the numerous other sharp reflections lying

out of the specular plane. Finally terfluorene films dewetted during annealing and no films suitable for X-ray scattering could be obtained.

Fig. 5 shows AFM images obtained in as-prepared and annealed pentafluorene films as well as in as-prepared terfluorene and heptafluorene films. The as-prepared pentafluorene film shows as low roughness and good flatness as the terfluorene and heptafluorene films. However, it can be seen that the annealing process led to a drastic texture change concomitant with the crystallization process of the pentafluorene film.

3.2 Absorption and photoluminescence properties in solution

Fig. 6 shows the absorption and steady-state PL spectra of the terfluorene, pentafluorene and heptafluorene in chloroform solution. The maximum absorption wavelength, maximum emission wavelength, the Stokes shift and the maximum molar extinction coefficient obtained from the spectra are listed in Table 1. The oligofluorene solutions are fully transparent in the visible range of wavelengths and are highly emissive in the blue region. Similarly to what has been previously reported in similar solvents, [32-35] the absorption spectra of these solutions display only one main peak at room temperature with no vibronic progression and they show a red-shift as the oligomer length is increased. As expected, the molar extinction coefficients reported in Table 1 are found to gradually increase with the number of fluorene units. However, the molar extinction coefficient *per* fluorene unit slightly increases with the oligomer length, which could suggest a little cooperative effect between fluorene units that modifies their individual oscillator strength. The PL spectra shown in Fig. 6 also indicate a red-shift of both the maxima of absorption and emission spectra upon increasing the oligomer length, which results from an extension of the π-conjugation length. As shown in Table 1, the Stokes shift decreases as the number of fluorene units and the conjugation length increase. Similar behavior has been observed in series of acene and phenyl oligomers and was attributed in these systems to a correlation between electron-vibrational coupling and oligomer length.[36]

PLQYs and PL decays were measured in the oligofluorene solutions to gain further insights into the photophysical properties of the materials. The PL decays in such solutions are monoexponential (data not shown) and the PL lifetimes were determined by fitting the data with a single exponential decay function. The measured values of the PLQYs and PL lifetimes are

listed in Table 1. The terfluorene, pentafluorene and heptafluorene solutions were found to exhibit PLQY values of 80, 82 and 90 %, respectively, indicating a trend of increasing the fluorescence efficiency with the oligomer length. In parallel, we can see a clear decrease of the PL lifetime with the oligomer length, ranging from 720 ps for the terfluorene to 490 ps for the heptafluorene. We then calculated the radiative and non-radiative decay rates, noted k_R and k_{NR}, respectively, from the values of the PLQY and the PL lifetime, by using the following equations:

$$PLQY = \frac{k_R}{k_R + k_{NR}}, \qquad \tau = \frac{1}{k_R + k_{NR}}. \tag{1}$$

The calculated k_R and k_{NR} values are listed in Table 1. The determination of the radiative decay rate allows us to calculate the transition dipole in fluorescence, noted $|d_f|$, using the following equation: [37-40]

$$\left|d_f\right|^2 = \frac{3\pi\varepsilon_0 \hbar^4 c^3 \left\langle E^{-3} \right\rangle}{n_0 \tau_R} \tag{2}$$

where ε_0 is the vacuum dielectric constant, $\hbar = h/2\pi$ is the Planck's constant, c is the speed of light, n_0 is the refractive index of the medium, taken here as that of the chloroform, $\tau_R = 1/k_R$ corresponds to the radiative lifetime and $\left\langle E^{-3} \right\rangle = \int E^{-3} I(E) dE / \int I(E) dE$ is calculated from the fluorescence intensity I(E) at the photon energy E. The d_f values in units of Debye are reported in Table 1. As expected, the radiative decay rate and the fluorescence transition dipoles in solution increase with the oligomer length. A previous work has studied the electronic absorption and fluorescence transitions in oligofluorenes of different lengths experimentally and using density functional theory (DFT).[41] While they found that the transition dipole in absorption follows an $n^{0.5}$ dependence on the number of fluorene units n, the transition dipole in fluorescence started to saturate for n>5. This important result was attributed to structural relaxation of the molecules in the excited state and indicated that localization of the excitation in the middle of the oligomer occurred in longer oligofluorenes. Our data are consistent with this previous report on

oligofluorenes and will be compared to the results obtained in films to provide new useful insights into the role of molecular conformation on the photophysical properties of oligofluorene films.

An overlap of the absorption and the PL spectra of the oligomers can be seen in Fig. 6. According to Förster energy transfer theory,[42] the energy transfer rate (k_{ET}) from a donor to the acceptor separated from each other by a spacing distance r is given by: $k_{ET} = (1/\tau_d)(R_0/r)^6$, where τ_d is the PL lifetime of the donor and R_0 is the Förster radius, which corresponds to the distance at which the rate of energy transfer equals the sum of all other rates for exciton relaxation. The Förster radius can be determined using the following equation:

$$R_0^6 = \frac{9000 \ln 10 \kappa^2 PLQY}{128 \pi^5 n_0^4 N_A} \int_0^\infty F_D(\lambda) \varepsilon_A(\lambda) \lambda^4 d\lambda \quad (3)$$

where κ is the orientational factor of 2/3 for a random directional distribution for the donor and acceptor molecules, N_A is the Avogadro's number, $F_D(\lambda)$ and $\varepsilon_A(\lambda)$ correspond to the normalized PL and molar extinction coefficient spectra. Using Eq.3, we calculated R_0 from the PL and absorption spectra of the oligofluorenes measured in solution. We found R_0 values of 1.2, 2.9 and 3.3 nm for the terfluorene, pentafluorene and heptafluorene, respectively, indicating that R_0 increases with the oligomer length. In good consistency with previous reports on exciton diffusion in fluorene derivatives,[35,39,43-45] these results suggest that singlet excitons can diffuse in the oligofluorene films by a Förster-type dipole-dipole coupling.

3.3 Electronic properties of the oligofluorenes

To examine the role of the oligomer length on the electronic properties of the oligofluorenes, quantum chemistry calculations were carried out to calculate the HOMO-LUMO gap energies and the frontier orbital distributions. For this purpose, the optimized geometries of the oligofluorene structures calculated at the B3LYP/6-311G(d,p) level are displayed in Fig. 7. We found that increasing the number of fluorene units in these optimized geometries do not modify significantly the inter-fluorene dihedral angles. Maps showing the 3D distributions of the calculated HOMOs and LUMOs are also displayed in Fig. 7. In the terfluorene, both the HOMO and LUMO are well distributed over the whole molecule. The HOMO and LUMO of the

pentafluorene are more localized in the three central fluorene units. As the number of fluorene units increases, this localization of the molecular frontier orbitals in the center of the molecules becomes more and more striking. These results are consistent with the picture of exciton self-trapping in the middle of the oligofluorenes.[41]

The HOMO and LUMO energies as well as the HOMO-LUMO energy gap were also calculated in the oligofluorenes of different lengths. The calculated values are plotted in Fig. 8 versus 1/n where n represents the number of fluorene units in the oligomer. While the absolute value of the HOMO energy level (E_{HOMO}) and the energy gap gradually decrease with the number of fluorene units, the absolute value of the LUMO energy level (E_{LUMO}) increases. In excellent agreement with a previous cyclic voltammetry study, we found that the HOMO and LUMO energy levels as well as the HOMO-LUMO energy gap follow linear relationships with the reciprocal number of fluorene units.[46] It is however important to emphasize that these findings were obtained either in solution and in the presence of an electrolyte or by quantum chemistry calculations. As described by Ishii et al.,[47] the ionization potential and electron affinity of an organic material in the solid-state are generally different from those of an isolated molecule due to some multielectronic effects. In addition, the ionization potential is different from the absolute value of the HOMO energy calculated using density functional theory (DFT) methods.[48] As a consequence, the behavior in films can be different from those found in solution or determined by quantum chemistry calculations. In that context, UPS is now a well-established experimental technique for measuring the ionization potential and thus the energy levels in organic thin films.[47-53] This technique will be used in the next section to provide further insights into the electronic properties of oligofluorenes in thin films.

3.4 Absorption and electronic properties of the as-prepared films

Fig. 9 presents the absorption spectra measured in pristine oligofluorene thin films. These films are highly transparent in the visible region and strongly absorb UV light. The absorption tail at wavelengths longer than 425 nm is presumably due to the reflection properties of the films.[35] For all the oligomers investigated in this work, two absorption peaks are observed. The absorption band at shorter wavelengths (200-250 nm) is nearly the same for all compounds and can be attributed to the π-π* electronic transition localized on the individual fluorene aromatic

unit. The absorption peak at longer wavelengths (300-425 nm) originates from the excitonic coupling between monomers [54] and is red-shifted when increasing the number of fluorene units and thus the oligomer length, as expected.[32-35] The optical energy gap (E_g), which was evaluated from the long-wavelength absorption edge, decreases from 3.07 to 2.87 eV with an increase of the oligofluorene length. In parallel, the quantum chemistry calculations led to HOMO-LUMO energy gaps varying from 3.83 eV for the terfluorene to 3.54 eV for the heptafluorene. It is well-known that the optical energy bandgap is generally different from the true gap because it does not take into account the Coulombic stabilization energy between the electron-hole pair and the polarization energies of the electron and the hole.[47]

The ionization potential (I_p) of the oligofluorene films was determined from the UPS spectra shown in Fig. 10a. The results indicate that the ionization potential values of the oligofluorene films lie between 5.56 and 5.78 eV. It is interesting to note that these values are different from the absolute values of the HOMO levels determined from the quantum chemistry calculations (ranging from 5.3 to 5.45 eV). This could be due to the fact that the absolute value of the HOMO energy level is often shifted with respect to the ionization energy. Koopmans' theorem which states that the vertical ionization potential is identical to the calculated absolute value of the HOMO energy is generally not satisfied because of relaxation processes during the ionization process and the electronic correlation. Although the optical bandgap differs as mentioned above from the true electronic gap, the electron affinity is generally approximated from the difference between the ionization potential and optical bandgap E_g values.[47,55-57] Using this method, the electron affinity of the oligofluorene films was found to yield approximated values in the range between 2.63 and 2.82 eV. The ionization potential and the electron affinity as well as the optical bandgap energies measured in the oligofluorene films are shown in Fig. 10b. In excellent consistency with the previous cyclic voltammetry measurements[46] and with the quantum chemistry calculations, these parameters present linear relationships with the reciprocal number of fluorene units.

3.5 Photoluminescence properties in as-prepared films

The fluorescence spectra of the as-prepared oligofluorene films excited at 350 nm are shown in Fig. 11. All the samples emit in the blue region of the spectrum with band shapes which do not markedly differ from those for the solutions. It should be noticed however that the spectra of the pristine films are about 5-6 nm red-shifted as compared to those in the solution.[58]

As expected, a red-shift of the emission is observed with the extension of the oligomer length. The wavelength of the emission maximum is indeed shifted from 399 nm for terfluorene to 423 nm for octafluorene. The spectra also exhibit similar vibronic structure with two peaks associated with the (0,0) and (0,1) transitions and a shoulder at longer wavelengths that can be assigned to the (0,2) transition. It is worth noting that an overlap between the absorption and the PL spectra of the oligofluorene films, suggesting that singlet excitons can migrate indeed in the film by Förster-type dipole-dipole coupling. However, the R_0 values cannot be accurately calculated in films because of the long tails on the absorption spectra above 425 nm which are due to reflection and scattering losses.

As displayed in Table 2, PLQY values of 45, 62 and 51% were measured in terfluorene, pentafluorene and heptafluorene thin films, respectively. They are consistent with the PLQYs previously reported in thin films made of other oligofluorene derivatives functionalized with different side chains.[26,59-61] These PLQY values are lower than those measured in solution, which indicates that a quenching of the emission occurs in the solid-state. Fig. 12 shows the PL kinetics of the oligofluorenes in thin films. The PL decays could be fitted by a single exponential decay function to determine a characteristic PL lifetime (τ). As shown in Table 2, PL lifetimes were measured to be 690, 800 and 680 ps in terfluorene, pentafluorene and heptafluorene, respectively. In contrast to the clear conjugation length dependence of the PLQY and PL lifetime observed in solution, the PLQY values and the PL lifetimes measured in the oligofluorene films did not show a trend as a function of the oligomer length. The highest PLQY and the longest PL lifetime were indeed obtained in pentafluorene thin film. The different behavior observed in solution and in thin films is likely to be due to intermolecular PL quenching or molecular conformational effects that can strongly affect the photophysical properties of the films. To clarify this issue, we then calculated the radiative and non-radiative decay rates, k_R and k_{NR}, respectively, from the measurements of the PLQY and the PL lifetime in films. The k_R and k_{NR} values, obtained using Eq.1, are listed in Table 2. The terfluorene film shows the slowest radiative decay rate constant with a value of 0.65×10^9 s^{-1}. Those measured in pentafluorene and heptafluorene films were found to be nearly identical with values of 0.78×10^9 and 0.75×10^9 s^{-1}, respectively. The transition dipole moments in fluorescence were then calculated in thin films using Eq. 2 and are also reported in Table 2. Values of 10, 11.2 and 11.1 Debyes were obtained in the as-prepared

terfluorene, pentafluorene and heptafluorene films, respectively. It is interesting to note that the k_R and d_f values in films are significantly lower than those measured in solution. It can also be seen that, in contrast to the results in solution, the radiative decay rate constant and d_f do not show a gradual increase with the oligomer length. A previous study has shown by a combination of DSC and solid-state NMR measurements that the oligofluorenes tend to adopt distinct molecular conformations according to the number of monomeric units.[31] A plausible explanation for our photophysical results is that the oligofluorenes of different lengths show various degrees of twisting between fluorene units in the solid-state and this could substantially affect the actual conjugation length of the molecules. Overall, our results suggest that the actual conjugation length is structurally dependent and, as a consequence, the oligomer chain length should be distinguished from the effective conjugation length in the oligofluorene films.

Regarding the non-radiative decay, the k_{NR} value of 0.47 x 10^9 s^{-1} obtained in the as-prepared pentafluorene film is significantly lower than those measured in terfluorene and heptafluorene films, which are in the order of 0.7-0.8 x 10^9 s^{-1}. It can also be seen that these rate constants in films are significantly higher than those determined in solution. Several processes can be involved in the non-radiative decay of light-emitting organic thin films including internal conversion to the ground-state, intersystem crossing to the triplet state, exciton-exciton annihilation and energy transfer to quenchers. Because our measurements were carried out at low excitation densities, no intensity dependence of the PL decays could be observed and we can neglect exciton-exciton interactions as well as quenching processes involving triplets and polarons.[62-68] In fact, the non-radiative decay rate in the oligofluorene thin films can be seen as a sum of the non-radiative deactivation rate of isolated molecules and the quenching rate due to intermolecular interactions. The intramolecular decay rate is often taken as the value of k_{NR} measured in solution where energy transfer to quenchers is much smaller. However, this assumption could not be valid for the oligofluorene films since the various degrees of twisting between fluorene units that affect the radiative decay rate could also have an influence on the intramolecular quenching processes. Evidently, intermolecular quenching processes should also be taken into account. Previous works on fluorene derivatives have described intermolecular quenching in terms of diffusion-mediated excitation energy transfer to quenchers.[35,39,43] In that framework, the intermolecular quenching rate is generally well-described by the Smoluchowski

equation[69] and depends on the singlet exciton diffusion processes and the concentration of quenching sites.[70] A complete characterization of the exciton diffusion processes in the oligofluorene films would be needed to evaluate the concentration of quenchers and clarify the role of the oligomer length on the exciton diffusion coefficient. Regarding the quenching sites in the oligofluorene films, their nature is still not elucidated but we can already exclude quenching by excimers and fluorenone defects since we did not observe any changes in the PL spectra and any spectral dependence of the fluorescence lifetime.[35,39,43] Overall, we found that the oligofluorenes show a stronger fluorescence quenching in films than in solution. Nevertheless, the PLQY of these films remains high with values ranging from 45 to 62 %. Our results also demonstrate that the lack of conjugation dependence in the PLQY and PL lifetimes of the as-prepared oligofluorene films are due to the higher radiative decay rate and the lower non-radiative decay rate constants measured in the pentafluorene film. This indicates that the pentafluorene derivative is particularly well suited for organic light-emitting applications.

3.6 Amplified spontaneous emission in as-prepared films

Fig. 13 shows the emission spectra measured from the edge of oligofluorene thin films for different pump excitation densities in the femtosecond regime. The thickness of the spin-coated films was 150 nm for terfluorene and 180 nm for pentafluorene and heptafluorene. All samples were placed in a nitrogen flow during these measurements. A spectral line narrowing was clearly observed at high pumping intensities, which is due to amplified spontaneous emission.[71-74] The full-width-at-half-maximum (FWHM) in all samples was found to drop to around 6 nm at high excitation densities. Amplification occurred at 423, 442 and 445 nm in terfluorene, pentafluorene and heptafluorene films, respectively. The red-shift of the ASE peak with the extension of the oligomer length is consistent with the shift observed in the steady-state fluorescence spectra. Note that the line narrowing effect in all our samples took place near the 0-1 vibronic transition of the steady-state fluorescence spectra, as expected for a quasi-four-level vibronic system.[17] Fig. 13 also shows the output light intensity detected from the edge of the oligofluorene films as a function of the excitation density. The abrupt variation in slope efficiency is directly related to the ASE threshold, which was measured to be 1.3, 1.2 and 0.4 $\mu J/cm^2$ in ter-, penta- and heptafluorene films, respectively. We also characterized the ASE

properties of oligofluorene films under ambient conditions. The terfluorene films placed in air did not display any ASE for excitation densities lower than 12 μJ/cm^2 and showed a fast degradation under laser irradiation, which suggests a significant oxidative quenching of the excited states in this material. On the other hand, the pentafluorene film was found to be more stable against photodegradation but exhibited higher ASE threshold than in inert atmosphere. Typical ASE threshold values measured in air were 5 μJ/cm^2 for pentafluorene and 8 μJ/cm^2 for heptafluorene. It is worth mentioning again that these ASE threshold values were obtained for femtosecond excitation pulses. Previous works investigating the ASE and lasing properties of fluorene derivatives mainly used nanosecond excitation pulses.[5,9,75] To be able to compare the performance of the pentafluorene used in this work with those of other fluorene based compounds, we also characterized the ASE properties of the film using a nanosecond pulsed Nd:YAG laser (pulse duration: 6-8 ns, repetition rate: 10 Hz). The ASE threshold of the pentafluorene film measured in air was found to be around 9 μJ/cm^2. This value is slightly lower than those previously reported in PFO and in a bisfluorene cored-dendrimer, which were measured in the nanosecond regime to be around 29 and 16 μJ/cm^2, respectively.[5,9]

Because photodegradation is a major issue concerning the application of organic materials for solid-state laser applications,[75-78] it is important to characterize the stability of the ASE properties of the oligofluorene films. The photostability was examined by monitoring the evolution of the emission output intensity from the edge of the films as a function of the irradiation time / incident pump pulse number. These measurements were performed with films placed either in ambient atmosphere or in a nitrogen flow. The samples were optically pumped by femtosecond pulses at a repetition rate of 5 kHz and with a pumping intensity in the range between 2.5 and 3 μJ/cm^2, which is near or above the ASE threshold. While no shift in the emission wavelength was observed, the output intensity was found to gradually decay with time as shown in Fig. 14. For all oligofluorene derivatives investigated here, the output decay curves were slower when the films were placed in the nitrogen flow, suggesting again that the photodegradation is faster in presence of oxygen. We evaluated the characteristic photostability lifetime of the output decay curves by measuring the irradiation time / number of incident pump pulses at which the emission intensity decays to half of its initial maximum value. Photostability lifetimes measured in air were found to be about 3.5 minutes (~1x10^6 pump pulses) and 40

seconds (~2 x 10^5 pump pulses), for the pentafluorene and the heptafluorene films, respectively. Under nitrogen flow, the photostability of the emission was improved and lifetimes of 45 seconds (2.25 x 10^5 pump pulses), 19.5 minutes (5.9 x 10^6 pump pulses) and 45 seconds (2.25 x 10^5 pump pulses) were measured in the terfluorene, pentafluorene and heptafluorene films, respectively. It should be mentioned that a recovery of the output intensity was not observed in any case. The results displayed in Fig. 14 provide clear evidence that the pentafluorene film presents the best photostability at high pumping intensities above the ASE threshold in both ambient and inert atmospheres. This finding is presumably related to the highest PLQY and the lowest non-radiative decay rate of the pentafluorene film, which can imply a significant reduction of the photobleaching of the material under laser irradiation. Direct comparison with results previously reported in the literature is not straightforward because of the different experimental conditions used to excite the films. Nevertheless, such a comparison suggests that the oligofluorenes used in this study, and especially the pentafluorene derivative, show a relatively good photostability at pumping intensities higher than the ASE threshold. For example, the photostability lifetime above the ASE threshold has been measured to be less than 31 x 10^3 pulses in perylene diimide derivatives,[79] around 10^4 pulses in spiro-quaterphenyl[80] and around 16 x 10^3 pulses in a PMMA host doped with a laser dye.[81] These values are substantially lower than those found in the oligofluorenes but were obtained in the nanosecond or picosecond regimes. It is also worth mentioning that the characteristic photostability lifetime measured in the oligofluorenes compare well to what has been reported in solid-state lasers, including those based on Alq_3-4-dicyanomethylene-6-(dimethylaminostyryl)-2-methyl-4H-pyran (DCM), with typical lifetime values of 10^5-10^6 pulses.[82,83] Overall, the low ASE thresholds, the straightforward tunability of the ASE wavelength upon tuning the oligomer length and the good photostability of the films at high pumping intensities provide evidence that these oligofluorenes are attractive candidates for organic solid-state laser applications.

3.7 Charge transport in as-prepared oligofluorene OFETs

Bottom-contact OFETs based on ter-, penta- and heptafluorene thin films were fabricated to investigate the charge transport properties of these materials. The thickness of the organic semiconducting layers was typically between 50 and 80 nm. The dielectric material consisted of a native SiO_2 layer and gold was used for the source/drain electrodes. The output and transfer

characteristics shown in Fig. 15 indicate that oligofluorene films operate as p-type semiconducting layers in the fabricated devices. No ambipolar transport was observed[13-15] which is presumably due either to the use of native SiO_2 as dielectric or to the large mismatch between the work function of source/drain gold electrodes and the LUMO level of the oligofluorenes, or both. The output curves show well-defined linear and saturation regions. Their behavior at low drain-source voltage (V_d) suggests that contact resistance effects occur between the organic layers and the gold source-drain electrodes. Hole field-effect mobility (μ_h) was determined from our device characteristics in the saturation regime using the standard method described elsewhere.[84] Threshold voltage (V_{th}), on/off current ratio ($I_{on/off}$) and μ_h values are listed in Table 2. The mobility values were measured to be 1.3×10^{-7}, 8.6×10^{-7} and 2.6×10^{-6} $cm^2\ V^{-1}\ s^{-1}$ in ter-, penta- and heptafluorene films, respectively. These values are lower than those reported in oligofluorene derivatives functionalized with shorter side chains.[28] These differences can be caused by the length of the side chains which presumably impacts on the transfer integral between neighboring molecular orbitals. Another reason could be simply the fact that the OFETs reported in this previous work were based on another device geometry. Indeed, that previous work used a bottom-contact top-gate architecture with a poly-chloro-p-xylylene gate dielectric layer.

More importantly, our results show that the field-effect mobilities increase with the length of the oligomer, which suggests a direct relationship between conjugation length and mobility in oligofluorene derivatives. Similar behavior has been observed in a series of oligofluorene-thiophenes in their crystalline state.[85] In contrast, hole and electron mobilities were found to decrease while increasing the oligomer length in a series of amorphous ambipolar oligofluorenes with C9 diaryl substitution.[86] While crystallinity and degree of molecular order presumably influence the oligomer length dependence of the charge carrier mobility, it is difficult to explain such different conjugation length dependences in amorphous thin films with similar local molecular environment. A plausible explanation would be that the distributions of the locations, orientations and conformations of molecules in the case of the currently studied oligofluorene films become more favorable for high charge carrier mobility as the conjugated backbone length increases. In contrast, thin films made of the longer oligofluorenes with C9

diaryl substitution could exhibit larger variation of molecular orientation/conformation and thus larger disorder, resulting in a decrease of the charge carrier mobilities.

3.8 Annealing effects in pentafluorene thin films

The XRD results reported in Fig. 4 have demonstrated a strong influence of a thermal annealing on the molecular packing in pentafluorene films. We were interested in examining the effects of this thermal treatment on the photophysical and charge transport properties. Fig. 16a shows the absorption spectra of pentafluorene in solution and in films before and after a thermal annealing at 100 ºC. It can be seen that the spectra in thin films are slightly red-shifted as compared to that in solution. More importantly, the as-prepared film shows an absorption peak with a maximum at 370 nm, while the annealed film exhibits two peaks located at 370 and 390 nm. It should also be pointed out that the film thickness strongly increases upon annealing, due to the concomitant molecular reorganization process. For instance, an as-prepared pentafluorene film with a thickness of 51 nm was found to show a thickness of 105 nm after treatment. As a consequence, while the absorption coefficient in the annealed films is close to that of the as-prepared films, the absorbance is significantly larger in the annealed samples.

As shown in Fig. 16b, the fluorescence spectra of pentafluorene in solution and in films before and after thermal annealing exhibit a similar vibronic structure. However, annealing the film leads to a 9 nm blue-shift of the emission. According to a theoretical study, the oligofluorenes in their ground-state are not planar, the interactions between adjacent fluorene units resulting in a twisted configuration with a 36º dihedral angle between successive monomers.[87] Similarly to what has been observed in a bisfluorene-cored dendrimer thin film,[88] the blue-shift of the emission spectrum of pentafluorene film upon annealing could be due to an increase of the dihedral angle between fluorene units. The apparent decrease of the (0,0) transition relative to the (0,1) transition in the emission spectrum of the annealed pentafluorene film can be explained by the fact that the short wavelengths of the emission spectrum overlap more strongly with the absorption spectrum, leading to partial reabsorption of the blue tail of the emission signal. It is also worth noting that the thermal treatment of the pentafluorene film does not lead to the greenish emission typically observed in polyfluorenes after annealing.[25]

The PLQY of the pentafluorene film was measured in the same sample before and after a thermal treatment at 100 ºC. As shown in Table 2, the PLQY was found to slightly increase from 62 to 65% upon annealing. In parallel, the PL lifetime obtained from the PL decays displayed in Fig.12 was found to decrease from 800 to 680 ps. These PL lifetimes are larger than that of 560 ps measured in the pentafluorene solution. From the PLQY and PL lifetime values, radiative and non-radiative decay rates of pentafluorene in annealed film were calculated using Eq. 1. The results obtained in the annealed film are summarized in the Table 2. Radiative decay rate of 0.96 x 10^9 s^{-1} was measured in annealed film. This indicates that annealing the pentafluorene film leads to a larger radiative decay rate than in the pristine sample, which was measured to be 0.78 x 10^9 s^{-1}. However, the radiative decay rates in both annealed and as-prepared films are lower than that in solution. Using Eq.3, the transition dipole moment in fluorescence of the annealed film was found to be around 12.4 D, which is higher than the value of 11.2 D measured in the pristine sample. We attribute the variations of k_R and d_f to changes in the conformation of the pentafluorene molecules, each of these conformations having supposedly different degrees of twisting between fluorene units. The non-radiative decay rate constant k_{NR} in annealed film was found to be 0.51 x 10^9 s^{-1}, which is similar to the value of 0.47 x 10^9 s^{-1} measured in pristine film. The lack of variations in the non-radiative decay rate upon thermal treatment indicates that the increase of crystallinity in the whole annealed pentafluorene film does not modify significantly its fluorescence quenching properties. This indicates that the effects of the thermal treatment on the photophysical properties of the pentafluorene films are essentially due to the changes in molecular conformations.

Fig. 16c shows the emission spectra measured from the edge of a pentafluorene film before and after thermal annealing for different pump excitation densities in the femtosecond regime. It can be seen that amplification occurs at 442 and 433 nm in the as-prepared and annealed films, respectively. The blue-shift of the ASE upon thermal treatment is consistent with that observed in the steady-state photoluminescence spectrum. The FWHM in both samples is found to drop to around 6 nm at high excitation intensities. ASE threshold of 1.2 $\mu J/cm^2$ was determined in the annealed pentafluorene film from the curve displayed in Fig. 16d. This value is similar to that evaluated in pristine film, which seems to be consistent with the similar PLQY values obtained in these films. Interestingly, the drastic change of the film structure and

morphology during the annealing process preserves its good ASE performance. The results demonstrate the possibility to finely tune the emission color of oligofluorene film without affecting its PLQY and ASE threshold, which is of potential interest for color adjustment of oligofluorene OLEDs and lasers without affecting their efficiencies.

The influence of thermal annealing on the charge transport properties of pentafluorene OFETs was also examined. Fig. 17 shows the output and transfer characteristics measured in the annealed device. The device parameters V_{th}, $I_{on/off}$ and μ_h, deduced from these curves, are summarized in Table 2. It can be seen that annealing leads to a reduction of V_{th} from -48 to -36 V and an increase of $I_{on/off}$ from 100 to 10^4. More importantly, we found that the charge carrier mobility after annealing increased from 8.6 x 10^{-7} to 3.8 x 10^{-5} cm^2 V^{-1} s^{-1}. This enhancement cannot be explained by the changes observed in HOMO and LUMO since the ionization potential measured by UPS slightly increases from 5.56 to 5.74 eV upon annealing. These changes should actually even result in the opposite observation, ie a less efficient hole injection from the gold electrodes after thermal treatment. In that context, we attribute the strong improvement of the charge carrier mobility to the increase of crystallinity evidenced by the XRD measurements. Noticeably, the mobility found in the annealed pentafluorene film is significantly higher than that evaluated in the as-prepared heptafluorene device, illustrating the necessity to improve the sample crystalline and to decrease the molecular disorder inside the crystals in order to enhance the charge transport properties of organic semiconducting thin films. Note that annealing the heptafluorene device at 100 ºC does not modify the amorphous character of the organic film and only slightly increases the hole mobility from 2.6 x 10^{-6} to 3.6 x 10^{-6} cm^2 V^{-1} s^{-1}, which is still one order of magnitude lower than that of annealed pentafluorene device.

There are already a number of reports where a same material shows differences in mobility of several orders of magnitude, depending on the morphology and the molecular packing of the organic semiconducting films.[89-95] The highest charge carrier mobilities are generally obtained in organic semiconducting films with few defects and with well-ordered and closely packed molecules.[95,96] Unfortunately, such morphologies often lead to strong intermolecular interactions and a quenching of the luminescence.[97] In that context, a trade off must be found in most cases between charge transport and photophysical properties for the

realization of high performance light-emitting devices. In many soft organic semiconducting materials, thermal annealing has been proven to be a successful approach to control the order and packing of the molecules in thin films.[98-101] In this work, we demonstrated the possibility in oligofluorene films to promote charge transport via an increase of the sample crystallinity without decreasing at the same time the fluorescence efficiency. Our results show indeed that thermal annealing of an amorphous pentafluorene film leads to a high degree of uniform and long-range molecular order which is locked by a cold crystallization. These features are responsible for the observed enhancement of the hole field-effect mobility by almost two orders of magnitude. In parallel, the photophysical properties of the pentafluorene, which depend more on the molecular conformations were not strongly modified. While little changes in the optical spectra and a decrease in the PL lifetime were observed, the PLQY was even slightly improved after annealing. All these findings demonstrate the importance of controlling the film morphology and molecular conformation to improve both the charge transport and the photophysical properties of oligofluorene films. Such a simultaneous improvement of charge carrier mobilities and PL efficiencies in low ASE threshold organic semiconducting materials is particularly relevant for future works on organic light-emitting devices and organic lasers. [17,102]

4. Conclusions

In summary, we have investigated the photophysical and charge transport properties of a series of solution-processable oligofluorenes in thin films and have evaluated their potential for organic solid-state laser applications. The results show the role played by the conjugation length on their optical spectra, HOMO/LUMO levels, PLQY and PL lifetimes, ASE properties and charge carrier mobilities. The low ASE thresholds (≤ 1.3 μJ/cm^2) together with the tunability of the ASE peak wavelengths spanning from 423 to 445 nm indicate that these materials are potentially attractive for optically-pumped organic solid-state laser applications. In relation with the cold recrystallization process in the bulk material, significant changes of the thin film morphology were evidenced during thermal annealing of the pentafluorene derivative, causing a blue-shift of the emission spectrum and ASE peak without noticeable variations in PLQY and ASE threshold. This behavior suggests the possibility of fine-tuning the color of pentafluorene light-emitting devices without any losses in efficiency with a single annealing step. In addition,

pentafluorene transistors showed an enhancement of the hole field-effect mobility by about two orders of magnitude after annealing. This improvement was attributed to the increase of crystallinity and long-range molecular order in the annealed film. Overall, this work provides useful information on the role of the conjugation length and film morphology on the photophysical and charge transport properties of oligofluorenes and should be taken into account in future works devoted to the development of fluorene derivatives for organic optoelectronic applications. In terms of applications, the low mobilities of the oligofluorenes used in this study may limit their potential use in electrically-driven organic optoelectronic applications. However, because of the tunability of their emission in the blue region of the spectrum and their low ASE threshold, these oligomers are extremely promising for organic photonic devices including optically-pumped organic solid-state lasers.

ACKNOWLEDGMENTS

This work has been carried out in the framework of the French-Korean International Laboratory "CNRS-EWHA Research Center for Ultrafast Optics and Nanoelectronics of Functional Nanostructures". The authors would like to acknowledge funding from "Campus France" (STAR program). JCR acknowledges the support by the Basic Science Researcher Program and the Quantum Metamaterials Research Center (QMMRC) through the National Research Foundation of Korea (NRF) funded by the Ministry of Education, Science and Technology (grants 2011-0008650, 2012-0000543). LM is thankful to French government for Polish-French "cotutelle" PhD program. L.M., K.M. and M.S. acknowledge the support of the Foundation for Polish Science under a Welcome grant "Organometallics in Nanophotonics". The authors are grateful to Dr. A. Muranaka from RIKEN and Mr. Y. Yokota from Yokohama National University for careful discussions and kind supports in the quantum chemistry calculations. We also thank Pohang Accelerator Laboratory (PAL) for giving us the opportunity to perform the GIWAXS measurements, MEST and POSTECH for supporting these experiments, Dr. Tae Joo Shin for adjustments and help, and other people from 9A U-SAXS beamline for assistance

REFERENCES

[1] R.H. Friend, R.W. Gymer, A.B. Holmes, J.H. Burroughes, R.N. Marks, C. Taliani, D.D.C. Bradley, D.A. Dos-Santos, J.L. Bredas, M. Logdlund and W.R. Salaneck, *Nature*, 1999, **397**, 121-128.

[2] C.C. Wu, Y.T. Lin, K.T. Wong, R.T. Chen and Y.Y. Chein, *Adv. Mater.*, 2004, **16**, 61-65.

[3] Q.B. Pei and Y. Yang, *J. Am. Chem. Soc.*, 1996, **118**, 7416-7417.

[4] J.P.J. Markham, E.B. Namdas, T.D. Anthopoulos, I.D.W. Samuel, G.J. Richards and P.L. Burn, *Appl. Phys. Lett.*, 2004, **85**, 1463.

[5] G. Heliotis, D.D.C. Bradley, G.A. Turnbull and I.D.W. Samuel, *Appl. Phys. Lett.*, 2002, **81**, 415.

[6] G. Heliotis, R. Xia, D.D.C. Bradley, G.A. Turnbull, I.D.W. Samuel, P. Andrew and W.L. Barnes, *Appl. Phys. Lett.*, 2003, **83**, 2118.

[7] C. Kamutsch, C. Gyrtner, V. Haug, U. Lemmer, T. Farrell, B.S. Nehls, U. Scherf, J. Wang, T. Weimann, G. Heliotis, C. Pflumm, J.C. deMello and D.D.C. Bradley, *Appl. Phys. Lett.*, 2006, **89**, 201108.

[8] T. Riedl, T. Rabe, H.H. Johannes, W. Kowalsky, J. Wang, T. Weimann, P. Hinze, B. Nehls, T. Farrell and U. Scherf, *Appl. Phys. Lett.*, 2006, **88**, 241116.

[9] J.C. Ribierre, G. Tsimimis, S. Richardson, G.A. Turnbull, I.D.W. Samuel, H.S. Barcena and P.L. Burn, *Appl. Phys. Lett.*, 2007, **91**, 081108.

[10] D. Amarasinghe, A. Ruseckas, A.E. Vasdekis, G.A. Turnbull and I.D.W. Samuel, *Adv. Mater.*, 2009, **21**, 107-110.

[11] S. Richardson, H.S. Barcena, G.A. Turnbull, P.L. Burn and I.D.W. Samuel, *Appl. Phys. Lett.*, 2009, **95**, 063305.

[12] Y. Yang, G.A. Turnbull and I.D.W. Samuel, *Adv. Funct. Mater.*, 2010, **20**, 2093-2097.

[13] L.L. Chua, J. Zaumseil, J.F. Chang, E.C.W. Ou, P.K.H. Ho, H. Sirringhaus and R.H. Friend, *Nature*, 2005, **434**, 194-199.

[14] C.C. Wu, T.L. Liu, W.Y. Hung, W.Y. Lin, K.T. Wong, R.T. Chen, Y.M. Chen and Y.Y. Chien, *J. Am. Chem. Soc.*, 2003, **125**, 3710-3711.

[15] H. Kaji, K. Koiwai, Y. Hirose and Y. Ohmori, *Org. Electr.*, 2010, **11**, 509-513.

[16] U. Scherf and E.J.W. List, *Adv. Mater.*, 2002, **14**, 477-487.

[17] I.D.W. Samuel and G.A. Turnbull, *Chem. Rev.*, 2007, **107**, 1272-1295.

[18] A.R. Buckley, M.D. Rahn, J. Hill, J. Cabanillas-Gonzales, A.M. Fox and D.D.C. Bradley, *Chem. Phys. Lett.*, 2001, **339**, 331-336.

[19] X. Gong, J.C. Ostrowski, G.C. Bazan, D. Moses, A.J. Hegger, M.S. Liu and A.K.Y. Jen, *Adv. Mater.*, 2003, **15**, 45-48.

[20] G. Tsiminis, J.C. Ribierre, A. Ruseckas, H.S. Barcena, G.J. Richards, G.A. Turnbull, P.L. Burn and I.D.W. Samuel, *Adv. Mater.*, 2008, **20**, 1940-1944.

[21] G. Tsiminis, A. Ruseckas, I.D.W. Samuel and G.A. Turnbull, *Appl. Phys. Lett.*, 2009, **94**, 253304.

[22] J.R. Lawrence, G.A. Turnbull, I.D.W. Samuel, G.J. Richards and P.L. Burn, *Opt. Lett.*, 2004, **29**, 869-870.

[23] A.J. Cadby, P.A. Lane, H. Mellor, S.J. Martin, M. Grell, C. Giebeler, D.D.C. Bradley, M. Wohlgennant, C. An and Z.V. Vardeny, *Phys. Rev. B*, 2000, **62**, 15604-15609.

[24] M. Grell, D.D.C. Bradley, G. Ungar, J. Hill and K.S. Whitehead, *Macromolecules*, 1999, **32**, 5810-5817.

[25] E.J.W. List, R. Guentner, P.S. de Freitas and U. Scherf, *Adv. Mater.*, 2002, **14**, 374-378.

[26] Y. Geng, S.W. Culligan, A. Trajkovska, J.U. Wallace and S.H. Chen, *Chem. Mater.*, 2003, **15**, 542-549.

[27] Y. Geng, A.C.A. Chen, J.J. Ou, S.H. Chen, K. Klubek, K.M. Vaeth and C.W. Tang, *Chem. Mater.*, 2003, **15**, 4352-4360.

[28] T. Yasuda, K. Fujita, T. Tsutsui, Y. Geng, S.W. Culligan and S.H. Chen, *Chem. Mater.*, 2005, **17**, 264-268.

[29] R. Anemian, J.C. Mulatier, C. Andraud, O. Stephan and J.C. Vial, *Chem. Comm.*, 2002, 1608-1609.

[30] M.J. Frisch, G.W. Trucks, H.B. Schlegel, G.E.Scuseria, M.A. Robb, J.R. Cheeseman, G. Scalmani, V. Barone, B. Mennucci, G.A. Petersson, H. Nakatsuji, M. Caricato, X. Li, H.P. Hratchian, A.F. Izmaylov, J. Bloino, G. Zheng, J.L. Sonnenberg, M. Hada, M. Ehara, K. Toyota, R. Fukuda, J. Hasegawa, M. Ishida, T. Nakajima, Y. Honda, O. Kitao, H. Nakai, T. Vreven, J.A. Montgomery, J.E. Peralta, F. Ogliaro, M. Bearpark, J.J. Heyd, E. Brothers, K.N. Kudin, V.N. Staroverov, T. Keith, R. Kobayashi, J. Normand, K. Raghavachari, A. Rendell, J.C. Burant, S.S. Iyengar, J. Tomasi, M. Cossi, N. Rega, J.M. Millam, M. Klene, J.E. Knox, J.B. Cross, V. Bakken, C. Adamo, J. Jaramillo, R. Gomperts, R.E. Stratmann, O. Yazyev, A.J. Austin, R. Cammi, C.

Pomelli, J.W. Ochterski, R.L. Martin, K. Morokuma, V.G. Zakrzewski, G.A. Voth, P. Salvador, J.J. Dannenberg, S. Dapprich, A.D. Daniels, O. Farkas, J.B. Foresman, J.V. Ortiz, J. Cioslowski and D.J. Fox, Gaussian 09, revision C.01; Gaussian, Inc.: Wallingford, CT, 2010.

[31] O.D. Bernardinelli, G.C. Faria, L.A. de Oliveira Nunes, R.M. Faria, E.R. de Azevedo and M.F.S. Pinto, *J. Phys. Chem. A* 2012, **116**, 4285-4295.

[32] J. Jo, C. Chi, S. Hoger, G. Wegner and D.Y. Yoon, *Chem. Eur. J.*, 2004, **10**, 2681-2688.

[33] C. Chi, C. Im and G. Wegner, *J. Chem. Phys.*, 2006, **124**, 024907.

[34] D. Wasserberg, S. P. Dudek, S.C.J. Meskers and R.A.J. Janssen, *Chem. Phys. Lett.*, 2005, **411**, 273-277.

[35] J.C. Ribierre, A. Ruseckas, P.E. Shaw, H.S. Barcena, P.L. Burn and I.D.W. Samuel, *J. Phys. Chem. C*, 2008, **112**, 20463-20468.

[36] L.O'Neill, P. Lynch, M. McNamara and H.J. Byrne, *Synth. Met.* 2005, **153**, 289-292.

[37] S.J. Strickler and R.A. Berg, *Chem. Phys.* 1962, *37*, 814.

[38] R.S. Knox and H. Van Amerongen, *J. Phys. Chem. B* 2002, *106*, 5289-5293.

[39] A.K. Bansal, A. Ruseckas, P.E. Shaw and I.D.W. Samuel, *J. Phys. Chem. C* 2010, **114**, 17864-17867.

[40] J.C. Ribierre, A. Ruseckas, H. Cavaye, H.S. Barcena, P.L. Burn and I.D.W. Samuel, *J. Phys. Chem. A* 2011, **115**, 7401-7405.

[41] S. Schumacher, A. Ruseckas, N.A. Montgomery, P.J. Skabara, A.L. Kanibolotsky, M.J. Paterson, I. Galbraith, G.A. Turnbull and I.D.W. Samuel, *J. Chem. Phys.* 2009, **131**, 154906.

[42] T. Förster, *Discuss. Faraday Soc.* 1959, **27**,7-17.

[43] J. C. Ribierre, A. Ruseckas, I.D.W. Samuel, H.S. Barcena and P.L. Burn, *J. Chem. Phys.*, 2008, **128**, 204703.

[44] R.Q. Albuquerque, C.C. Hofmann, J. Köhler and A. Köhler, *J. Phys. Chem. B* 2011, **115**, 8063-8070.

[45] M.A. Stevens, C. Silva, D.M. Russel and R.H. Friend, *Phys. Rev. B* 2001, **63**, 165213.

[46] C. Chi and G. Wegner, *Macromol. Rapid Commun.*, 2005, **26**, 1532-1537.

[47] H. Ishii, K. Sugiyama, E. Ito and K. Seki, *Adv. Mater.* 1999, **11**, 605-625.

[48] R. Kar, J.-W. Song, K. Hirao, J. Comput. Chem. 2013, 34, 958-964.

[49] J.C. Ribierre, S. Watanabe, M. Matsumoto, T. Muto, A. Nakao and T. Aoyama, *Adv. Mater.* 2010, **22**, 4044-4048.

[50] J.C. Ribierre, T. Fujihara, S. Watanabe, M. Matsumoto, T. Muto, A. Nakao and T. Aoyama, *Adv. Mater.* 2010, **22**, 1722-1726.

[51] J.C. Ribierre, T. Aoyama, S. Watanabe, J. Gu, T. Muto, M. Matsumoto, A. Nakao, T. Wada, *Jap. J. Appl. Phys.* 2010, **49**, 01AB06.

[52] N. Koch, A. Kahn, J. Ghijsen, J.J. Pireaux, J. Schwartz, R.L. Johnson and A. Elschner, *Appl. Phys. Lett.* 2003, **82**, 70.

[53] E.L. Bruner, N. Koch, A.R. Span, S.L. Bernasek, A. Kahn and J. Schwartz, *J. Am. Chem. Soc.* 2002, **124**, 3192-3193.

[54] R. Fortrie, R. Anémian, O. Stephan, J.-C. Mulatier, P.L. Baldeck, C. Andraud and H. Chermette, *J. Phys. Chem. C* 2007, **111**, 2270-2279.

[59] Y. Geng, A. Trajkovska, D. Katsis, J.J. Ou, S.W. Culligan and S.H. Chen, *J. Am. Chem. Soc.*, 2002, **124**, 8337-8347.

[60] D. Katsis, Y.H. Geng, J.J. Ou, S.W. Culligan, A. Trajkovska, S.H. Chen and L.J. Rothberg, *Chem. Mater.*, 2002, **14**, 1332-1339.

[61] J.U. Wallace and S.H. Chen, *Adv. Polym. Sci.*, 2008, **12**, 152.

[62] P.E. Shaw, A. Ruseckas and I.D.W. Samuel, *Adv. Mater.* 2008, **20**, 3516-3520.

[63] A.J. Lewis, A. Ruseckas, O.P.M. Gaudin, G.R. Webster, P.L. Burn and I.D.W. Samuel, *Org. Electr.* 2006, **7**, 452-457.

[64] A. Ruseckas, J.C. Ribierre, P.E. Shaw, S.V. Staton, P.L. Burn and I.D.W. Samuel, *Appl. Phys. Lett.* 2009, **95**, 183305.

[65] J.C. Ribierre, A. Ruseckas, K. Knights, S.V. Staton, N. Cumpstey, P.L. Burn and I.D.W. Samuel, *Phys. Rev. Lett.* 2008, **100**, 017402.

[66] J.C. Ribierre, A. Ruseckas, I.D.W. Samuel, S.V. Staton and P.L. Burn, *Phys. Rev. B* 2008, **77**, 085211.

[67] J. Kalinowski, W. Stampor, J. Mezyk, M. Cocchi, D. Virgili and P. Di Marco, *Phys. Rev. B* 2002, **66**, 235321.

[68] H.Y. Shin, J.H. Woo, M.J. Gwon, M. Barthelemy, M. Vomir, T. Muto, K. Takaishi, M. Uchiyama, D. Hashizume, T. Aoyama, D.W. Kim, S. Yoon, J.-Y. Bigot, J.W. Wu and J.C. Ribierre, Phys. Chem. Chem. Phys. 2013, 15, 2867-2872.

[69] Electronic Processes in Organic Crystals and Polymers, 2nd ed.; M. Pope and C.E. Swenberg, Eds.:Oxford University: Oxford, 1999.

[70] J.C. Ribierre, S.G. Stevenson, I.D.W. Samuel, S.V. Staton and P.L. Burn, *J. Displ. Technol.* 2007, **3**, 233-237.

[71] M.D. McGehee, R. Gupta, S. Veenstra, E.K. Miller, M.A. Diaz-Garcia and A.J. Heeger, *Phys. Rev. B*, 1998, **58**, 7035-7039.

[72] F. Hide, M.A. Diaz-Garcia, B.J. Schwartz, M.R. Andreson, Q.B. Pei and A.J. Heeger, *Science*, 1996, **273**, 1833-1835.

[73] G.J. Denton, N. Tessler, M.A. Stevens and R.H. Friend, *Adv. Mater.*, 1997, **9**, 547-550.

[74] C. Zenz, W. Graupner, S. Tasch, G. Leising, K. Mullen and U. Scherf, *Appl. Phys. Lett.*, 1997, **71**, 2566.

[75] R. Xia, G. Heliotis, Y. Hou and D.D.C. Bradley, *Org. Electr.* 2003, **4**, 165-177.

[76] G. Heliotis, R. Xia, D.D.C. Bradley, G.A. Turnbull, I.D.W. Samuel, P. Andrews and W.L. Barnes, *J. Appl. Phys.* 2004, **96**, 6959-6965.

[77] S. Stagira, M. Zavelani-Rossi, M. Nisoli, S. DeSilvestri, G. Lanzani, C. Zenz, P. Mataloni and G. Leising, *Appl. Phys. Lett.* 1998, **73**, 2860.

[78] S. Richardson, O.P.M. Gaudin, G.A. Turnbull and I.D.W. Samuel, *Appl. Phys. Lett.* 2007, **91**, 261104.

[79] E. M. Calzado, J.M. Villalvilla, P.G. Boj, J.A. Quintana, R. Gomez, J.L. Segura and M.A. Diaz-Garcia, *J. Phys. Chem. C* 2007, **111**, 13595-13605.

[80] N. Johansson, J. Salbeck, J. Bauer, F. Weissortel, P. Broms, A. Andersson and W.R. Salaneck, *Adv. Mater.* 1998, **10**, 1136-1140.

[81] A. Costela, I. Garcia-Moreno and R. Sastre, *Phys. Chem. Chem. Phys.* 2003, **5**, 4745-4763.

[82] V. Navarro-Fuster, E.M. Cazaldo, P.G. Boj, J.A. Quintana, J.M. Villalvilla, M.A. Diaz-Garcia, V. Trabadelo, A. Juarros, A. Retolaza and S. Merino, *Appl. Phys. Lett.* 2010, **97**, 171104.

[83] V.G. Kozlov, V. Bulovic, P.E. Burrows, M. Baldo, V.B. Khalfin, G. Parthasarathy, S.R. Forrest, Y. You and M.E. Thompson, *J. Appl. Phys.* 1998, **84**, 4096-4108.

[84] J. Zaumseil and H. Sirringhaus, *Chem. Rev.*, 2007, **107**, 1296-1323.

[85] H. Meng, J. Zheng, A.J. Lovinger, B.C. Wang, P.G. Van Pattern and Z. Bao, *Chem. Mater.*, 2003, **15**, 1778-1787.

[86] C.C. Wu, T.L. Liu, W.Y. Hung, T.H. Ke, K.T. Wong and T.C. Chao, *Appl. Phys. Lett.*, 2004, **85**, 1172.

[87] I. Franco and S. Tretiak, *Chem. Phys. Lett.*, 2003, **372**, 403-408.

[88] J.C. Ribierre, A. Ruseckas, O. Gaudin, I. D. W. Samuel, H. S. Barcena, S. V. Staton and P. L. Burn, *Org. Electr.*, 2009, **10**, 803-808.

[89]R. Schmidt, M.M. Ling, J.H. Oh, M. Winckler, M. Konemann, Z. Bhao and F. Wurthner, *Adv. Mater.* 2007, **19**, 3692-3695.

[90] M. O'Neill and S.M. Kelly, *Adv. Mater.* 2011, **23**, 566-584.

[91] L. Mazur, A. Castiglione, K. Ocytko, F. Kameche, R. Macabies, A. Ainsebaa, D. Kreher, B. Heinrich, B. Donnio, S. Sanaur, E. Lacaze, J.L. Fave, K. Matczyszyn, M. Samoc, J.W. Wu, A.J. Attias, J.C. Ribierre, F. Mathevet, *Org. Electr.* 2014, **15**, 943-953.

[92] Y. Diao, B.C.K. Tee, G. Giri, J. Xu, D.H. Kim, H.A. Becerril, R. M. Stoltenberg, T.H. Lee, G. Xue, S.C.B. Mannsfeld and Z. Bao, *Nature Mater.* 2013, **12**, 665-671.

[93] R. Noriega, J. Rivnay, K. Vandewal, F.P.V. Koch, N. Stingelin, P. Smith, M.F. Toney and A. Salleo, *Nature Mater.* 2013, **12**, 1038-1044.

[94] A. Facchetti, *Nature Mater.* 2013, **12**, 598.

[95] I. McCulloch, M. Heeney, C. Bailey, K. Genevicius, I. MacDonald, M. Skhunov, D. Sparrowe, S. Tierney, R. Wagner, W. Zhang, M.L. Chabinyc, R.J. Kline, M.D. McGehee and M.F. Toney, *Nature Mater.* 2006, **5**, 328-333.

[96] H. Sirringhaus, P.J. Brown, R.H. Friend, M.M. Nielsen, K. Bechgaard, B.M.W. Langeveld-Voss, A.J.H. Spiering, R.A.J. Janssen, E.W. Meijer, P. Herwig and D.M. de Leeuw, *Nature* 1999, **401**, 685-688.

[97] I.F. Perepichka, D.F. Perepichka, H. Meng and F. Wudl, *Adv. Mater.* 2005, **17**, 2281-2305.

[98] M. Funihashi, *Polym. J.* 2009, **41**, 459-469.

[99] H. Lino and J. Hanna, *Opto-electron. Rev.* 2005, **13**, 295-302.

[100] S. Sergeyev, W. Pisula and Y.H. Geerts, *Chem. Soc. Rev.* 2007, **36**, 1902-1929.

[101] P.A. Levermore, R. Jin, X. Wang, J.C. De Mello, and D.D.C. Bradley, *Adv. Funct. Mater.* 2009, **19**, 950-953.

[102] B.K. Yap, R. Xia, M. Campoy-Quiles, P.N. Stavrinou and D.D.C. Bradley, *Nature Mater.* 2008, **7**, 376-380.

Figure captions

Fig. 1

Chemical structures of the oligofluorenes used in this study

Fig. 2

Differential scanning calorimetry thermograms of pentafluorene (a), terfluorene (b) and heptafluorene (c). The first heating runs are the top curves recorded at 10 or 20°C/min. Further heating curves were recorded at rates of 20, 10, 5 and 2 °C/min (from top to bottom)

Fig. 3

X-ray diffractograms in the specular plane of as-prepared and annealed pentafluorene and heptafluorene thin films (a and c). Powder X-ray diffractograms of bulk as-prepared and annealed pentafluorene (b). Annealing temperature was 100 ºC.

Fig.4

Grazing incidence X-ray scattering patterns of as-prepared (a) and annealed (b) pentafluorene thin films. Annealing temperature was 100 ºC.

Fig. 5

50 x 50 μm AFM images measured in terfluorene, as-prepared and annealed pentafluorene and heptafluorene thin films. Annealing temperature was 100 ºC.

Fig.6

Normalized absorption and fluorescence spectra of the oligofluorenes in chloroform solution.

Fig.7

Optimized geometries, HOMO and LUMO frontier orbital distributions obtained at the B3LYP/6-311G(d,p) level

Fig.8

HOMO and LUMO energies as well as the HOMO-LUMO energy gap of the oligofluorenes calculated at the B3LYP/6-311G(d,p) level plotted against the reciprocal number of fluorene units (1/n).

Fig. 9

Absorption spectra of the oligofluorene thin films. The curves are normalized at 215 nm.

Fig. 10

(a) UV photoelectron spectra of oligofluorene thin films. (b) Correlation of the optical energy gap (E_g), ionization potential (I_p) and electron affinity (E_A) in the solid-state with the reciprocal number of fluorene units (1/n).

Fig. 11

Normalized fluorescence spectra of oligofluorene thin films. The excitation wavelength was 350 nm.

Fig. 12

Photoluminescence decays of the oligofluorenes in thin films. The solid lines correspond to the fits obtained from a single exponential decay function.

Fig. 13

(a) Amplified spontaneous emission (ASE) spectra at different light pumping intensities in as-prepared terfluorene film. The black line corresponds to the photoluminescence steady-state spectrum. (b) Emission intensity collected from the edge of terfluorene waveguiding thin films, integrated over all wavelengths versus the light pump intensity. The excitation wavelength of the femtosecond pump laser was 325 nm. (c) and (d) Results obtained in as-prepared pentafluorene film. (e) and (f) Results obtained in as-prepared heptafluorene film

Fig. 14

Normalized emission intensity versus pump irradiation time/number of pump pulses for as-prepared oligofluorene films in (a) ambient atmosphere and (b) in nitrogen atmosphere. The films were optically pumped by femtosecond pulses at a repetition rate of 5 kHz and with a pumping intensity in the range between 2.5 and 3 $\mu J/cm^2$.

Fig. 15

Output and transfer characteristics measured in OFETs based on terfluorene [(a) and (b)], pentafluorene [(c) and (d)] and, heptafluorene [(e) and (f)] as-prepared thin films.

Fig. 16

Panels (a), (b) and (c) show the influence of a thermal annealing at 100 ºC on the normalized absorption spectrum, the steady-state emission spectrum and the amplified spontaneous emission spectrum of a pentafluorene film, respectively. Absorption and PL spectra of the pentafluorene in

chloroform solution are also shown in (a) and (b). Panel (d) shows the emission intensity collected from the annealed pentafluorene film versus the light pump intensity.

Fig. 17

(a) Output and (b) transfer characteristics measured in an annealed pentafluorene OFET.

Table 1

Maximum absorption wavelengths (λ_{abs}), maximum emission wavelengths (λ_{em}), PLQYs, fluorescence lifetimes (τ_{sol}), radiative and non-radiative decay rates (k_R) and (k_{NR}), fluorescence transition dipole moment (d_f), Stokes shift, maximum molar extinction coefficients and Förster radius (R_0) measured in chloroform diluted solutions.

	λ_{abs} (nm)	λ_{em} (nm)	PLQY (%)	τ_{sol} (ns)	k_R (x 10^9 s^{-1})	k_{NR} (x 10^9 s^{-1})	d_f (Debye)	Stokes shift (cm^{-1})	ε ($L.mol^{-1}.cm^{-1}$)	R_0 (nm)
terfluorene	352	395	80	0,72	1.11	0.28	13.5	3092,6	72400	1.2
pentafluorene	370	412	82	0,56	1.46	0.32	16.3	2755,2	158500	2.9
heptafluorene	376	414	90	0,49	1.83	0.18	18.5	2441,2	225000	3.3

Table 2

PLQYs, fluorescence lifetimes, radiative and non-radiative decay rates (k_R) and (k_{NR}), fluorescence transition dipole moment (d_f), ASE thresholds, hole field-effect mobilities (μ_h), threshold voltages (V_{th}) and on/off current ratio ($I_{on/off}$) measured in oligofluorene derivatives.

	PLQY (%)	τ (ps)	k_R ($x10^9$ s^{-1})	k_{NR} ($x10^9$ s^{-1})	d_f (Debye)	ASE threshold ($\mu J/cm^2$)	μ_h (cm^2/Vs)	V_{th} (V)	$I_{on/off}$
Terfluorene	45	690	0.65	0.8	10	1.3	1.3×10^{-7}	-53	10^3
Pentafluorene (as-prepared)	62	800	0.78	0.47	11.2	1.2	8.6×10^{-7}	-48	10^2
Pentafluorene (annealed)	65	680	0.96	0.51	12.4	1.2	3.8×10^{-5}	-36	10^4
Heptafluorene	51	680	0.75	0.72	11.1	0.4	2.6×10^{-6}	-61	10^5

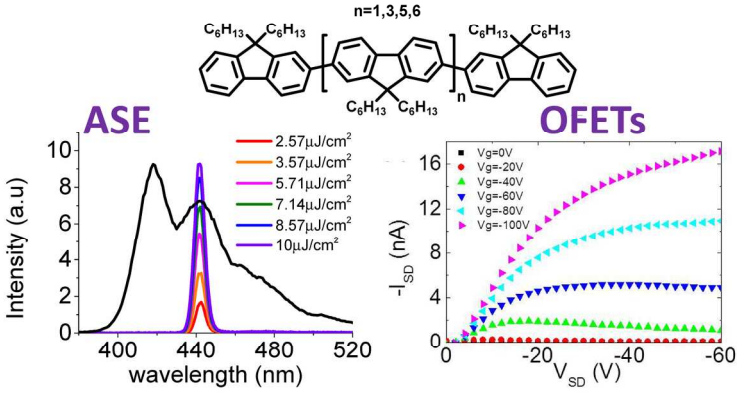

Graphical abstract
180x135mm (300 x 300 DPI)

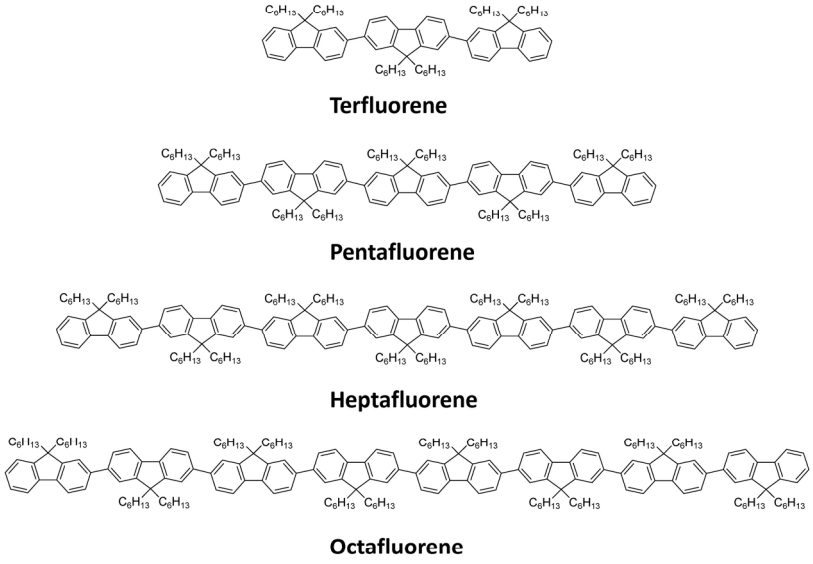

Figure 1
180x135mm (300 x 300 DPI)

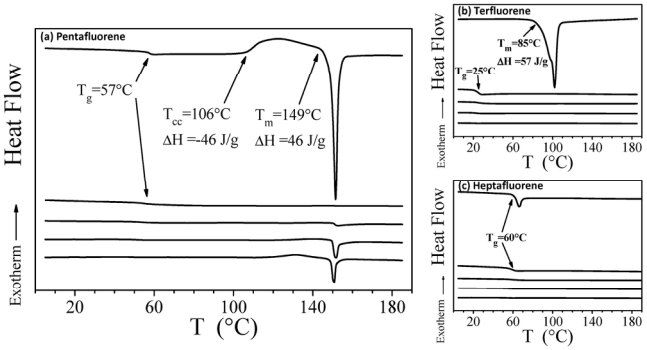

Figure 2
180x135mm (300 x 300 DPI)

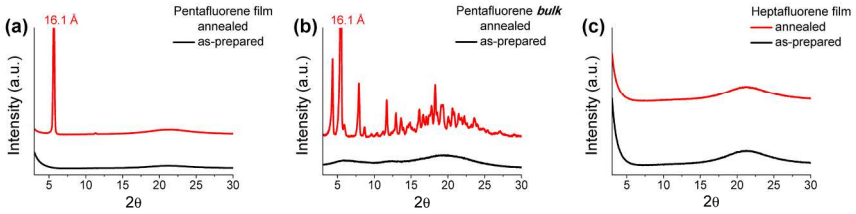

Figure 3
209x148mm (300 x 300 DPI)

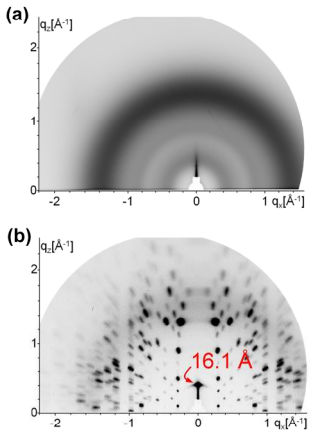

Figure 4
209x148mm (300 x 300 DPI)

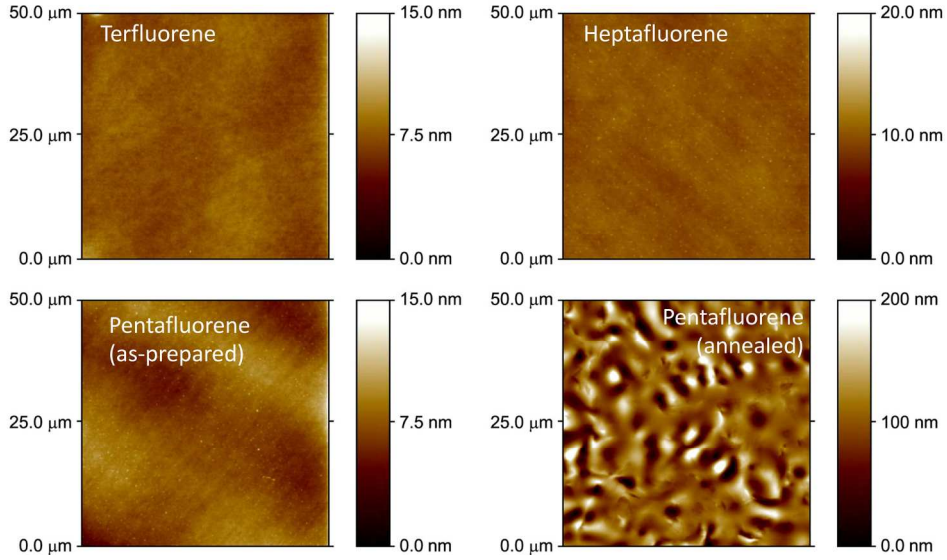

Figure 5
180x135mm (300 x 300 DPI)

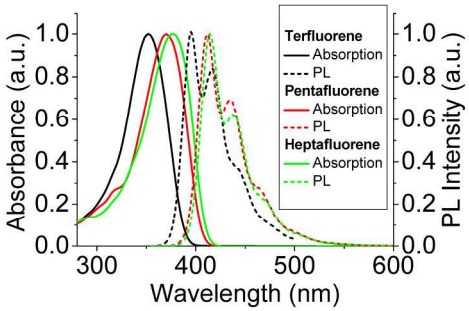

Figure 6
209x148mm (300 x 300 DPI)

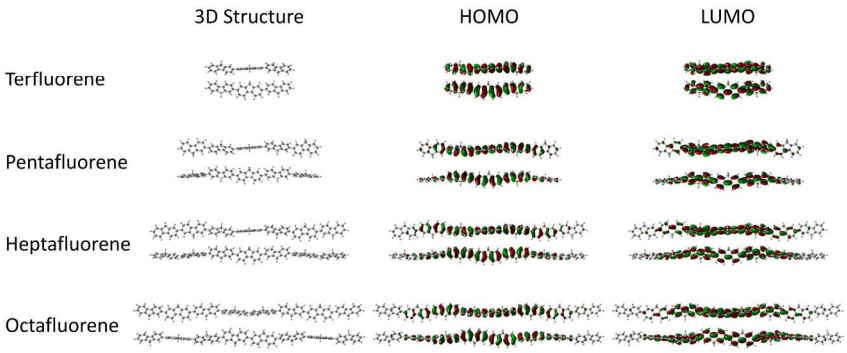

Figure 7
209x148mm (300 x 300 DPI)

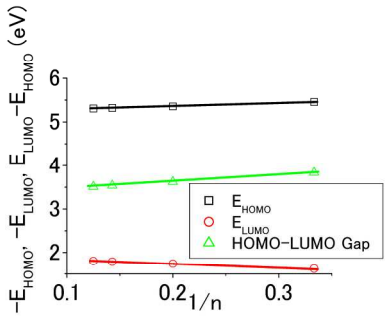

Figure 8
209x148mm (300 x 300 DPI)

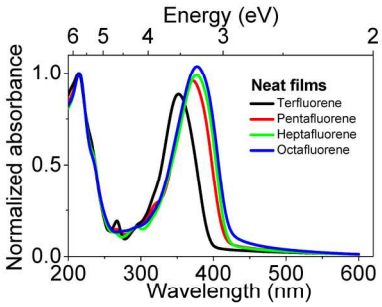

Figure 9
180x135mm (300 x 300 DPI)

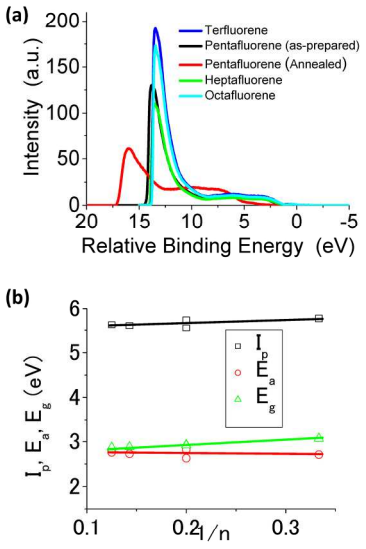

Figure 10
209x148mm (300 x 300 DPI)

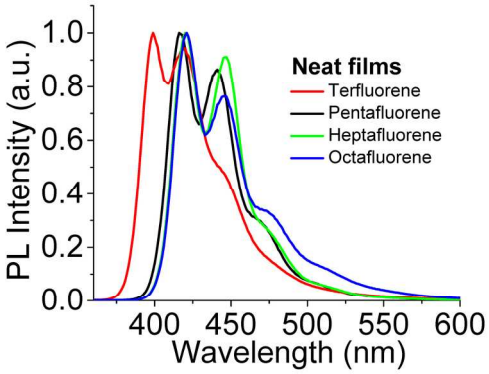

Figure 11
180x135mm (300 x 300 DPI)

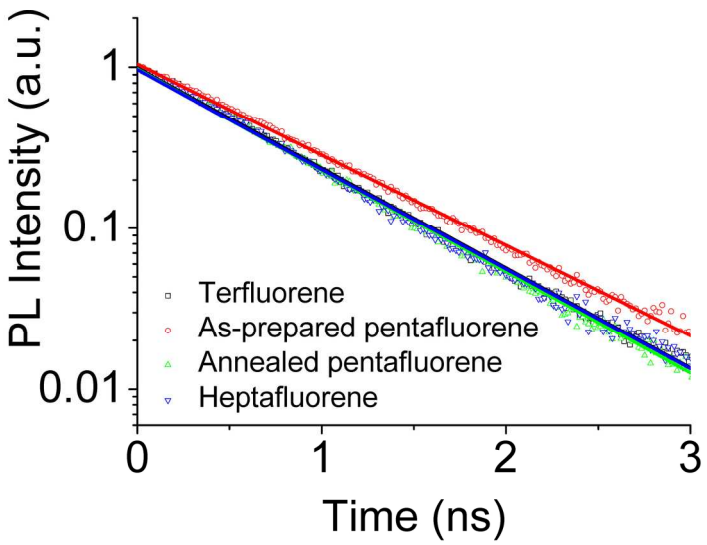

Figure 12
180x135mm (300 x 300 DPI)

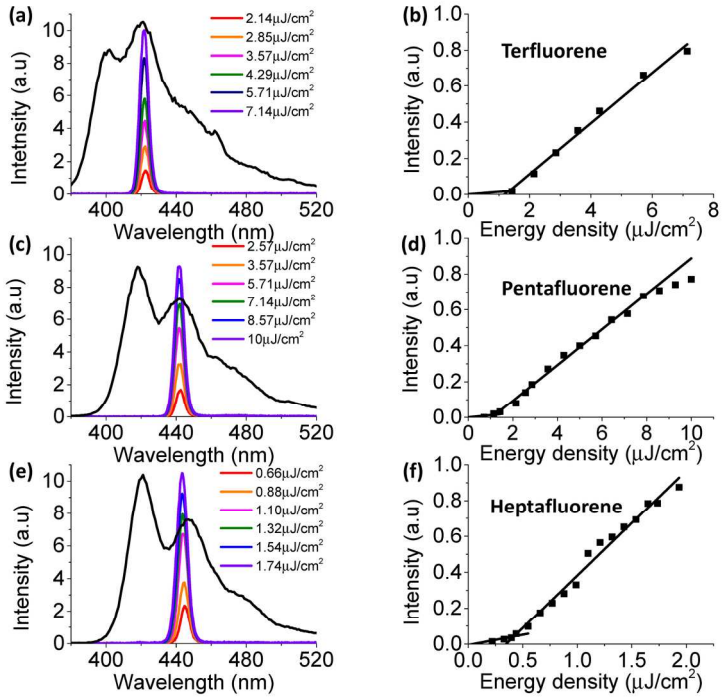

Figure 13
180x135mm (300 x 300 DPI)

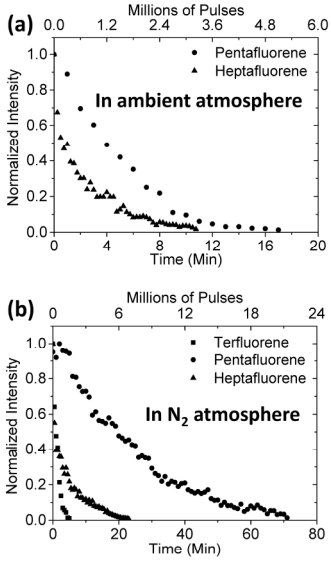

Figure 14
209x148mm (300 x 300 DPI)

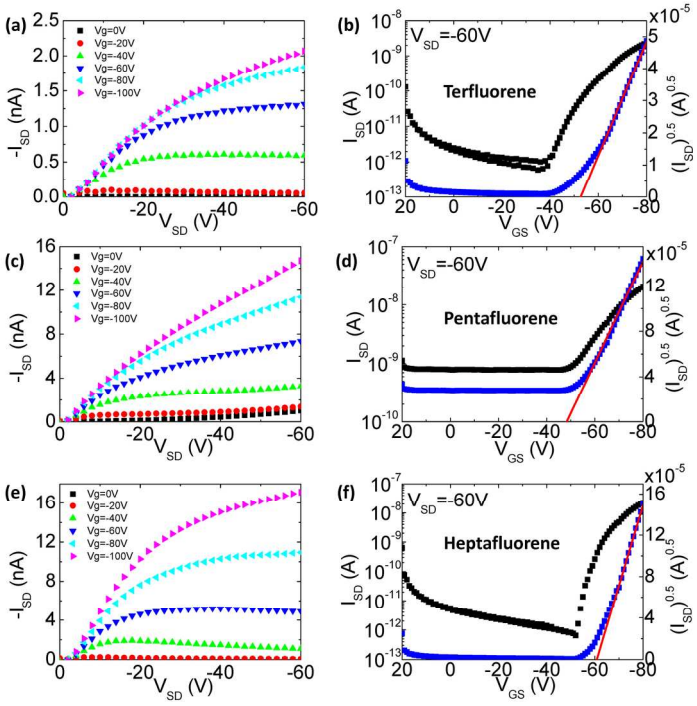

Figure 15
180x135mm (300 x 300 DPI)

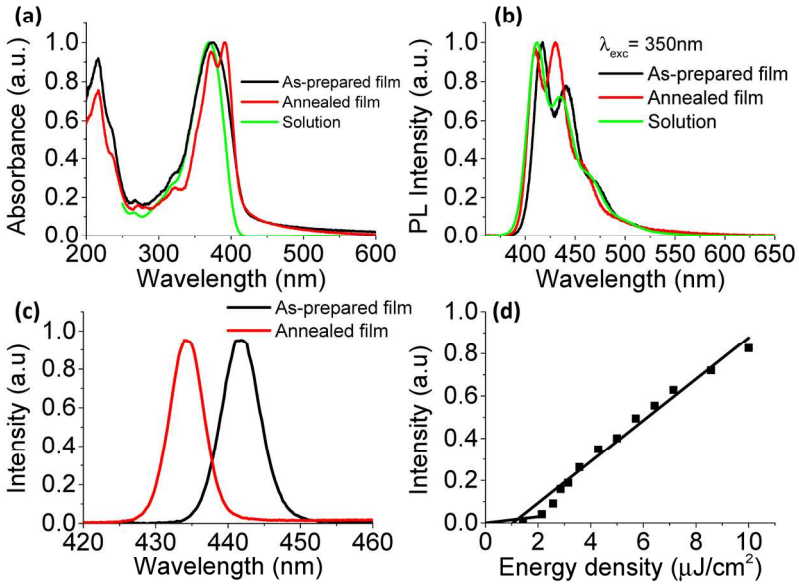

Figure 16
180x135mm (300 x 300 DPI)

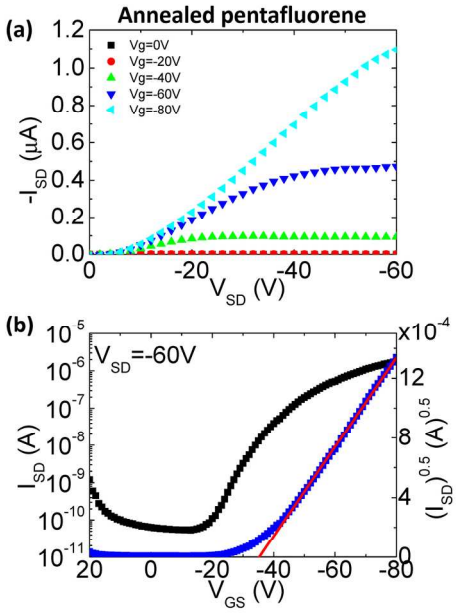

Figure 17
180x135mm (300 x 300 DPI)